Dipole-exchange propagating spin-wave modes in metallic ferromagnetic stripes

M. P. Kostylev,[1,2] G. Gubbiotti,[3] J.-G. Hu,[1,4] G. Carlotti,[3,5] T. Ono,[6] and R. L. Stamps[1]
[1]*School of Physics M013, University of Western Australia, 35 Stirling Highway, Crawley, Western Australia 6009, Australia*
[2]*Fachbereich Physik, Technische Universität Kaiserslautern, Kaiserslautern D-67663, Germany*
[3]*CNISM, Dipartimento di Fisica, Università di Perugia, Via A. Pascoli, I-06123 Perugia, Italy*
[4]*Department of Physics, Yangzhou University, Yangzhou 225002, People's Republic of China*
[5]*INFM-CNR Research Center S3, Via Campi 213/a, 41100 Modena, Italy*
and Dipartimento di Fisica, Universitá di Perugia, Via A. Pascoli, 06123 Perugia, Italy
[6]*Institute for Chemical Research, Kyoto University, Uji, Kyoto 611-0011, Japan*
(Received 12 July 2006; revised manuscript received 4 July 2007; published 13 August 2007)

Results from Brillouin light scattering experiments on guided spin waves propagating along metallic magnetic stripes are presented and analyzed. The spin waves propagate along the stripe axis and form mode families due to geometrical confinement in the stripe geometry. In consequence, the allowed wave vectors are quantized in the transverse directions by stripe width and height. We show that each standing spin-wave resonance across the stripe width is associated with a particular guided mode. In the case of stripes magnetized along their length, the group velocity of the guided modes is negative and all modes have a volume character. When the stripes are magnetized along their width, the modes are characterized by a positive group velocity, and the spectrum consists of a series of volume and localized modes.

DOI: 10.1103/PhysRevB.76.054422 PACS number(s): 75.30.Ds, 75.40.Gb, 76.50.+g

I. INTRODUCTION

The fundamental magnetic excitations in metallic ferromagnets typically have frequencies in the microwave region. The associated wavelengths are long, and the excitations can be thought of as classical spin waves. Spin waves are characterized by a variety of features that can be tuned through sample geometry, propagation direction, and applied magnetic fields. These characteristics make spin waves particularly useful for applications to spin-wave logic,[1,2] microwave frequency interferometry, and microwave signal processing technologies.[3] Moreover, spin waves are also excited during the switching of magnetic memory elements[4] and contribute significantly to noise associated with high-frequency applications. From the point of view of applications, one of the most interesting geometries is the magnetic stripe, defined as a very long magnetic rod with rectangular cross section.

Brillouin light scattering (BLS) technique experiments have, to date, probed only spin-wave resonances with the plane of incidence of light always perpendicular to the stripes.[5–10] These resonances exist as standing waves across the stripe width and are referred to here as WSSWR modes. The internal static magnetic field $\mathbf{H}_i$ and the equilibrium magnetization $\mathbf{M}_o$ are spatially homogeneous when the magnetization is along the stripe axis, as shown in Fig. 1(a). This alignment is the magnetic easy direction for soft magnets. In this geometry the magnetostatic surface wave will be quantized to form a WSSWR family.[6]

When the external field is applied transverse to the stripe axis in the direction of the stripe width and parallel to the incidence plane of light, as shown in Fig. 1(b), the $\mathbf{H}_i$ and $\mathbf{M}_o$ fields are inhomogeneous due to the stripe edges. This results in a very different spectrum of modes, consisting of a set of standing wave resonances and a limited number of localized modes.[7] The localized modes are excitations with magnetostatic energies due primarily to inhomogeneous fields existing near the stripe lateral edges. The resonances are formed by width quantization of Damon and Eshbach volume modes.[12] This mode is termed the "backward volume magnetostatic mode" because of its negative group velocity. In thin metallic films the spectrum of this mode is significantly affected by the exchange interaction. In particular, the dispersion of this type of mode is nonmonotonic.[13]

In addition to standing spin-wave resonances, propagating modes have been studied as collective excitations of densely packed periodic arrays of elements.[14–16] The collective modes are formed from WSSWRs in individual stripes coupled by long ranged dipole fields. These excitations exist for in-plane propagation perpendicular to the stripe axes. In what follows we term this the "transverse direction."

In the present paper we demonstrate that a type of propagating mode can exist in individual stripes and stripe arrays that is very different from the above transverse direction WSSWRs. Here we report BLS measurements made with the incidence plane, and consequently the spin-wave propagation direction, parallel to the stripe axes. We show that WSSWRs observed for this geometry are the long wavelength limit of a general class of guided spin wave modes that are distinct from the transverse WSSWR.

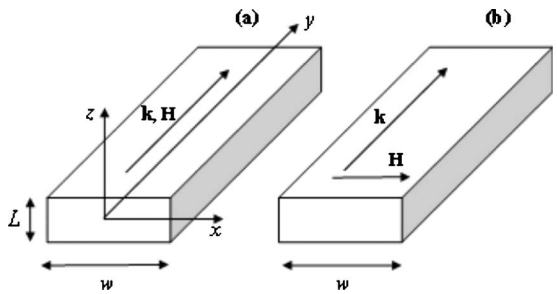

FIG. 1. Geometry of the sample: (a) longitudinal magnetization and (b) transverse magnetization.

The remainder of the paper is organized as follows. A description of the experimental results is given in the next section. Theoretical considerations are outlined in Sec. II with mathematical details contained in the Appendix. The paper concludes with a discussion in Sec. III and a short summary conclusion in Sec. IV.

II. EXPERIMENT

The excitations described above were studied experimentally with an applied static field **H** aligned along y for a "longitudinal magnetization," [as depicted in Fig. 1(a)] and for the field along x for a "transverse magnetization" [as depicted in Fig. 1(b)].

Permalloy ($Ni_{81}Fe_{19}$) stripes having thickness $L=30$ nm and width $w=600$ nm were prepared on thermally oxidized Si substrates by means of e-beam lithography, electron-gun deposition, and lift-off process. The stripes were arranged in a 1×1 mm^2 array with edge-to-edge spacing of 500 nm. For this spacing the elements can be considered noninteracting.

Brillouin light scattering measurements were carried out at the GHOST laboratory (University of Perugia). Monochromatic P-polarized light from a solid state laser ($\lambda=532$ nm) with a power of about 200 mW was focused on the patterned area using a camera objective of f-2 and focal length 50 mm. Cross-polarized, backscattered light was analyzed using a Sandercock type (3+3)-pass tandem Fabry-Pérot interferometer.[17]

In order to probe spin waves having a nonvanishing wave-vector component along the stripe length, the yz plane (see Fig. 1) was chosen as the plane of incidence of light. BLS spectra were recorded by varying θ, the incidence angle of the laser with respect to the sample normal, in the range $\theta=8°-70°$. This corresponds to changing the spin-wave wave-number component $k_y=(4\pi/\lambda)\sin\theta$ parallel to the stripe longitudinal axis y from 0.33×10^5 to 2.22×10^5 rad/cm. Important for this geometry is uncertainty in the value of the spatial Fourier component of dynamic magnetization along the x direction because of the stripe confinement in the "transverse" direction.[6] This uncertainty results in a considerable BLS cross section, especially at small incidence angles, from a number of guided modes with nonvanishing transverse wave numbers k_x.

Values for the saturation magnetization $4\pi M_S$ (9500 G) and the gyromagnetic ratio $\gamma/(2\pi)$ (2.82 MHz/Oe) were derived from fits to measured Damon-Eshbach mode frequencies as a function of spin-wave wave number in the unpatterned part of the film.[12] These values are assumed to apply also for the patterned regions.

Example BLS spectra for the case of longitudinal magnetization, with $H=1$ kOe along the y axis, are shown in Fig. 2(a). At any incidence angle one can observe several distinct peaks in the BLS spectra. Three frequencies decrease on increasing k_y, as shown in Fig. 3, upper panel. Note that the lowest-frequency peak has the largest BLS intensity, regardless of the angle of incidence.

The BLS spectra for the transverse stripe magnetization, with **H** along the x axis, are shown in Fig. 2(b). In this case a strong static field of 2.9 kOe was applied in order to ensure that most of the stripe volume was magnetized to saturation. Two families of modes are clearly seen in the figure. One set of modes corresponds to intensity peaks at frequencies above 10 GHz. The maximum BLS intensity in this family corresponds to the peak with the highest frequency. Modes of a second type exist at lower frequencies, where two overlapping sets of intensities can be detected. Note that with the scale of Fig. 2(b) it is difficult to see that the broad response at 6–8 GHz actually consists of two peak intensities. At an incidence angle of 10°, the higher frequency peak at 8 GHz has a larger BLS intensity than the peak at 16 GHz. As can be seen in the upper panel of Fig. 4, the frequencies of all peaks grow when the incidence angle θ is increased.

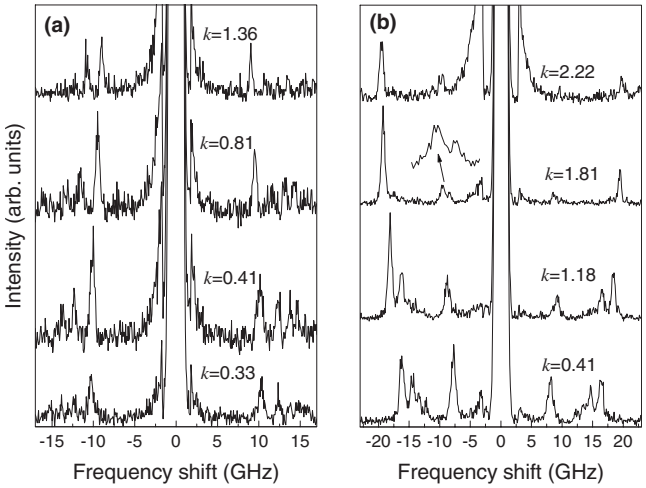

FIG. 2. Sequence of measured Brillouin scattering spectra. (a) Geometry of Fig. 1(a) and (b) geometry of Fig. 1(b). Spectra are recorded for different values of the transferred in-plane wave number (k_y) expressed in 10^5 cm^{-1}. An enlarged portion of the spectra showing the doublet is also shown.

One can also see a significant asymmetry in Stokes and anti-Stokes peaks for this configuration: the negative frequency instensities shown in Fig. 2(b) are considerably larger than the positive frequency intensities. The asymmetry increases with k_y. On the contrary, in Fig. 2(a) one sees that the asymmetry is noticeably smaller, and seems to decrease with increasing k_y.

III. THEORY

Early calculations for magnetostatic spin-wave propagation were made for insulating monocrystalline yttrium iron garnet ferrite films (see Ref. 18 and references therein). Spin-wave frequency dispersions in lengthwise magnetized metallic stripes were later calculated in Ref. 19 neglecting the inhomogeneous exchange interaction, and in Ref. 20 with account taken of dipolar and exchange contributions. It was shown that spin waves propagating along a metallic magnetic stripe appear as a set of guided width modes with discrete values of transverse wave numbers.

In the present work we use an approach valid for small stripe aspect ratios $p=L/w$. For $p\ll1$ it is natural to divide the set of width modes into families which differ by the

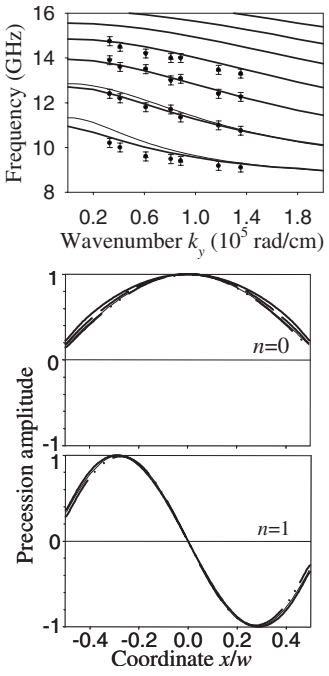

FIG. 3. Upper panel: frequency dispersion of guided spin-wave modes of a longitudinally magnetized Permalloy stripe [geometry in Fig. 1(a)]. Dots: experimental points. Thick lines: solution of Eq. (3), thin lines: two lowest modes from Eq. (13) in Ref. 11 with EBC from Ref. 25. Parameters of calculation: $w=600$ νm, $L=30$ nm, $4\pi M_S=9500$ G, $A=10^{-6}$ erg/cm, external field is 1000 Oe. Lower panels: modal distributions of dynamic magnetization for two lowest modes $n=0$ and $n=1$. Solid line: $k_y=0$, dashed line: $k_y=1\times10^5$ rad/cm, and dash-dotted line: $k_y=2\times10^5$ rad/cm. The thin solid line: EBC from Ref. 25. (Practically not seen, since very close to $k_y=2\times10^5$ rad/cm curve.) The value of the effective pinning parameter Ref. 25 calculated with the parameters of experimental sample (above) $d=14.9$. The surface anisotropy constant entering the expression for d was assumed to be zero. The error bars show the experimental error margins: ±200 MHz.

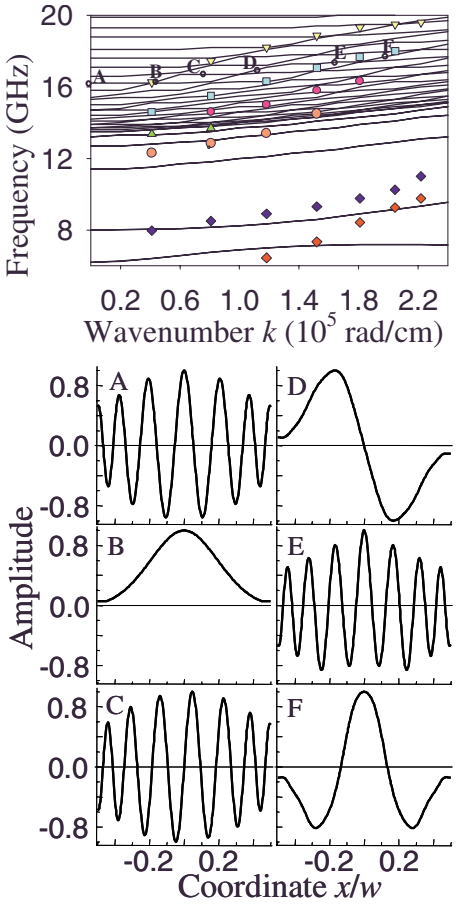

FIG. 4. (Color online) Upper panel: frequency dispersion of width modes of a transversely magnetized magnetic stripe [geometry in Fig. 1(b)]. External magnetic field is 2900 Oe. Other parameters are as in Fig. 3. Symbols (triangles, squares, circlces, etc.): experiment. Solid lines: calculation. The five lowest modes are edge-localized modes and the higher frequency modes span across the stripe width. Lower panels: modal distributions of dynamic magnetization for the points A, B, C, E, and F in the upper panel. The vertical size of the symbols shows the experimental error margins: ±200 MHz.

number of nodes of the standing wave across the smallest cross-sectional dimension. In our case the smallest stripe dimension is the film thickness. Depending on the magnetization direction, the lowest frequency family of width modes is formed by quantization of the Damon-Eshbach surface wave in the x direction in our geometry, with the applied field **H** directed along the x axis. For the applied field aligned along the y axis, the lowest frequency backward volume wave and high-order "standing spin waves" (SSWs) are quantized by the stripe width. The latter represent higher-order "thickness" modes for in-plane continuous metallic films, in the sense that they have nodes along the z axis.

In a continuous metallic film with thickness L lower than 40 nm, as in the present case, the frequency of the first SSW is usually shifted by the exchange interaction upwards, far away from the frequency range of the magnetostatic surface wave. The frequency of the first SSW is also shifted out of the range of frequencies of the lowest backward volume wave in the case of transverse magnetization. Consequently there are no degeneracies, leading to repulsions, of width modes in the lowest family with the width modes of the higher-order families. This is in contrast to observations made for modes in YIG films.[21]

In the calculations which follow, we make a simplifying assumption. For stripes patterned from thin metallic films, it is possible to accurately describe the spectrum of the lowest frequency modes by including exchange and neglecting the dipolar coupling to higher frequency families of high-order modes. This approximation is valid for the majority of stripe geometries of interest experimentally. Unless the stripe aspect ratio p is of order unity, exchange is the main contribution to the high-frequency families of modes. The exchange interaction eliminates hybridization between mode families by separating families in frequency due to the high-energy associated with the exchange stiffness for high-order mode families. This separation in frequency makes dipolar coupling of families nonresonant and inefficient.

In our mode family decoupling approximation, we average the dipole fields associated with spin waves across the

film thickness. This procedure makes contributions from the high-order families to the dynamic dipole fields of low frequency modes negligible. This method was first developed for unpatterned films where it was termed the "diagonal approximation," and was put on mathematically rigorous grounds in Ref. 22.

The averaging produced a simple one-dimensional Green's function describing the dipole field for WSSWRs. The validity of the approach for stripes was shown in[8] through a comparison with results obtained from an exact two-dimensional numerical calculation. This approximation slightly underestimates the frequencies of the lowest mode family. This error is negligible because the exact mode profiles in the z direction for the lowest family are very uniform across the film thickness. Note that in our approach, exchange energy contributions to the in-plane propagation are properly taken into account. Lastly, we note that our theory is applicable to a longitudinally or transversely magnetized stripe. Although not shown explicitly below, uniaxial magnetocrystalline anisotropy is also allowed in our numerical implementation.

We begin with an equation of motion for the magnetization based on the Landau-Lifschitz equation

$$\partial m/\partial t = -|\gamma|\{[\mathbf{M}_0(x,z)+\mathbf{m}(x,y,z,t)]\times[\mathbf{H}_i(x,z)+\mathbf{h}_d(x,y,z,t)+\mathbf{h}_{\mathrm{exc}}(x,y,z,t)]\}, \tag{1}$$

where $\mathbf{M}_0$ is the equilibrium magnetization, $\mathbf{H}_i$ is the static internal field, $\mathbf{m}$ is the dynamic magnetization, $\mathbf{h}_d$ is the dynamic dipole field induced by the dynamic magnetization, $\mathbf{h}_{\mathrm{exc}}$ is the effective dynamic exchange field associated with spatially inhomogeneous motion of magnetization, and γ is the gyromagnetic ratio. In a continuum approximation,

$$\mathbf{h}_{\mathrm{exc}}(x,y,z,t) = \alpha\nabla^2\mathbf{m}(x,y,z,t), \tag{2}$$

where $\alpha = A/2\pi M_S^2$, A is the exchange stiffness, and M_S is the value of saturation magnetization of the sample.

Following the method in Ref. 23 we derive an approximate Green's function describing the dipole field produced by the time varying components of the magnetization. The Green's function is valid in the limit $p \ll 1$. We assume that the dynamic magnetization and the dipole field represent a traveling wave along the y axis with negligible variation of dynamic magnetization and its dipole field along z, i.e.,

$$\mathbf{m}(x,y,z,t) = \mathbf{m}_k(x)\exp[i(k_y y-\omega t)],$$

$$\mathbf{h}_d(x,y,z,t) = \mathbf{h}_{dk}(x)\exp[i(k_y y-\omega t)]. \tag{3}$$

The dynamic demagnetizing field is

$$\mathbf{h}_{dk}(x) = 4\pi\int_{-w/2}^{w/2}\hat{G}_k(x-x')\mathbf{m}_k(x')dx', \tag{4}$$

where

$$G_{zzk}(s) = -\int_0^\infty\left(\frac{1}{a}-\frac{1}{b}\right)\frac{\cos(k_y t)}{\pi L}dt,$$

$$G_{xxk}(s) = -\int_0^\infty\frac{1}{b^4}\left[t^2(a-b)-\frac{p^2s^2}{a}\right]\frac{\cos(k_y t)}{\pi L}dt-\delta(s),$$

$$G_{yyk}(s) = -\delta(s)-G_{xxk}(s)-G_{zzk}(s),$$

$$G_{yxk}(s) = -G_{xyk}(s) = -\int_0^\infty\frac{2i}{b^2}\left[b-a-\frac{L^2}{a}\right]ts\frac{\sin(k_y t)}{\pi L}dt. \tag{5}$$

In the above expressions, $b=\sqrt{s^2+t^2}$, $a=\sqrt{b^2+L^2}$, and $\delta(s)$ is the Dirac delta function. Derivation and the properties of the Green's function (5) are given in the Appendix.

We linearize Eq. (1) using the conditions $|\mathbf{m}| \ll |\mathbf{M}_0| = M_S$, $|\mathbf{h}_d+\mathbf{h}_{\mathrm{exc}}| \ll |\mathbf{H}_i| = H_i$ and use Eqs. (2), (4), and (5). In the case of Fig. 1(b) $\mathbf{H}_i$ and $\mathbf{M}_o$ are spatially inhomogeneous. We neglect their variation across the film thickness which is reasonable for $p \ll 1$.[11] We arrive at an integrodifferential equation for the dynamic magnetization $\mathbf{m}_k(x)$,

$$-i\frac{\omega}{\gamma}\mathbf{m}_k(x) = \mathbf{m}_k(x)\times\mathbf{H}_i(x)+4\pi\mathbf{M}_o(x)\times\left[\alpha(\partial^2/\partial x^2-k_y^2)\mathbf{m}_k(x)+\int_{-w/2}^{w/2}\hat{G}_k(x-x')\mathbf{m}_k(x')dx'\right]. \tag{6}$$

One sees from Eq. (6) that the factor $-i\omega/\gamma$ plays the role of an eigenvalue of the tensorial integrodifferential operator on the right-hand side of Eq. (6).

IV. DISCUSSION

The system of equations described by Eq. (6) were solved numerically in order to determine the frequency dispersion $\omega(k_y)$. Results are shown by solid lines in the upper panel of Fig. 3 for guided modes with the external static magnetic field applied along the y axis. There is a good agreement with the measured experimental points. First one notices that with the increase in the longitudinal wave number k_y the eigenfrequency decreases, as expected for this family of modes which are based upon magnetostatic backward volume modes. Similar features were found in the earlier exchange-free calculation.[19] Indeed the closed form for G_{zzk} obtained in Ref. 24 shows that the out-of-plane component of the dipole field decreases with k_y. Our analysis shows that the same is valid for G_{xxk} (see Appendix), therefore the dipole energy of guided waves for longitudinally magnetized stripes decreases with k_y.

In the lower panels of Fig. 3 we show mode amplitude profiles calculated from the eigenfunctions satisfying Eqs. (6). The profiles are shown at example k_y values, calculated as eigenfunctions of the integro differential operator. The

profiles are represented by the m_{xk} amplitude plotted as a function of x. It is interesting to compare this numerical result with the approximate analytical method of effective boundary conditions (EBC) at the stripe edges $x=0,w$ suggested by Guslienko *et al.*[25] From the lower panels in Fig. 3 one sees that the magnetization profiles do not vary much with longitudinal wave number. One also sees that the mode profile is not strongly affected by k_y at large mode numbers. The profile should be harmonic and satisfy EBC at the stripe edges for $k_y=0$ according to the EBC theory. Such a profile is shown by a thin solid line in the panels, and is very similar to the numerically found profiles obtained from Eqs. (6). This justifies use of the effective boundary conditions[25] for arbitrary values of k_y. We note that this approximation was also made in Ref. 11 for spin waves on magnetic elements with a finite length in the y direction.

The thin solid lines in the upper panel show the dispersion of two lowest guided modes calculated using an analytical approximation wherein one quantizes the modes as described by Eq. (13) from Ref. 11. One sees a considerable discrepancy between the numerical results obtained from the present theory, as well as the experimental results, for the lowest frequency mode and at small values of wave number. Finally, it is also worth noting that the use of effective boundary conditions at the stripe edges in the form of the entirely pinned spins[21] results in a still larger discrepancy.

Figure 4 contains the results of the numerical solution of Eq. (6) with the external static field aligned transversely along the stripe width in the x direction. To treat the inhomogeneity of $\mathbf{H}_i$, an approximation originally due to Schlömann was used [Eq. (21) in Ref. 11]. Note that the Schlömann's formula is the limiting case $k_y=0$ of the integral (4) involving the Green's function (5) and a special shape of magnetization profile $\mathbf{m}_k(x)=\mathbf{e}_x$, where $\mathbf{e}_x$ is a unit vector along x.

The frequency spectrum in this transverse field case displays a rich and complex structure. First we note that the group velocity of the modes is positive. This can be understood as follows. Suppose that the magnetization were completely uniform, and define an in-plane wave vector $\mathbf{k}_{\text{in}}=k_y\mathbf{e}_y+k_x\mathbf{e}_x$. The orientation of $\mathbf{k}_{\text{in}}$ rotates from parallel to perpendicular to $\mathbf{H}_i(x)$ as k_y is increased. This rotation increases the mode frequency in the same manner that the Damon-Eschbach surface mode frequency increases with change in propagation direction due to magnetostatic energies.[12]

Note that $\mathbf{H}_i(x)$ is not uniform because of edge effects, and this results in the appearance of new low-frequency modes localized at the stripe edges. In Fig. 4 we see that the frequencies of the localized modes with $k_y=0$ coincide with the frequencies of localized WSSWRs found in Refs. 7 and 11. In this regard, the frequencies for the second type of intensites discussed earlier in reference to Fig. 2(b) are located close to the calculated frequencies for these localized modes. There is considerable discrepancy between measured and calculated frequencies because of our assumption of uniform static magnetization and local internal fields in the stripes. The exact distribution of magnetization and local fields will be strongly affected by edge morphology, defects, and history of magnetization.

The dense band of modes extending to higher frequencies in Fig. 4 consists of volume modes which represent WSSWRs of volume magnetostatic waves for $k_y=0$.[12] In the external field range 0–3 kOe, the magnetostatic volume waves for thin films have a much weaker dispersion than the magnetostatic surface wave. In the stripe geometry, quantization of the modes occurs due to confinement and results in a dense spectrum of WSSWRs and guided modes. The effect of the dipole interaction on the dispersion is small, and the influence of the exchange interaction is more pronounced than what one finds for a magnetostatic surface wave propagating on an unstructured film. The dipole energy decreases with increasing wave number, whereas the exchange contribution to the magnetic energy increases.[13] In unpatterned films this competition results in a minimum in the dispersion for volume modes. Such a dispersion quantized by confinement results in an entangled set of WSSWRs, in which the frequencies of the lowest volume resonances are situated between, and separated by, much higher volume WSSWRs.[7,11] Rotation of $\mathbf{k}_{\text{in}}$ from parallel to perpendicular to the static increases the frequency of spin waves in an unpatterned film. One can therefore expect crossing and repulsion of width mode frequencies in the patterned, confined geometry as mode degeneracies are encountered. Mode repulsion will be in fact accentuated by the confined geometry since the internal static field is inhomogeneous, leading to stronger hybridization.

One sees that experimental data shown in Fig. 4 fall along calculated frequencies where the group velocity is largest. The agreement between experiment and theory is best for the two high-frequency sets of experimental points (down triangles and squares). The next lowest frequency set of experimental points (circles) is offset by more than the experimental error (±200 MHz) from the theoretical curves. Regardless, one can clearly see that the experimental data follow nearby theoretical curves. As discussed above, this is probably due to assumptions in the model concerning static internal fields and magnetization.

Schlömann's static internal field model [Eq. (21) in Ref. 11], in combination with the magnetic parameters obtained from fitting the spin dispersion law measured on the unpatterned part of the sample, is in good agreement with the measured data for the high frequency intensity peaks. A detailed model for the static local fields and magnetization would be required in order to describe accurately frequencies of all volume modes.

Our calculation shows that mode hybridization is small in regions where the group velocity is largest. Consequently the profiles of dynamic magnetization are not strongly affected in these regions. Furthermore, we have verified that only modes with symmetric profiles contribute to measurable peaks in BLS spectra, and modes with antisymmetric profiles do not give a noticeable BLS signal (for example, see profile D in the lower panel of Fig. 4). For instance, the maximum BLS cross section in Fig. 2(b), indicated by triangles, is associated with the lowest symmetric mode corresponding to profile B in the lower panel of Fig. 4. The next strongest response (indicated by squares) is associated with a two node symmetric mode (profile F in Fig. 4). One would expect that the next contribution to the BLS signal should be from the

symmetric mode having four nodes in the dynamic magnetization profile. Indeed, from the upper panel in Fig. 4 we see that most of the data are sandwiched between two bounds: the upper bound corresponding to the antisymmetric mode with three nodes, and the lower bound corresponding to the symmetric mode with four nodes.

The maximum intensity for the lowest-frequency peak in the case of the longitudinal wire magnetization [shown in Fig. 2(a)] may be understood similarly, because this mode is the lowest-frequency mode with even symmetry.

We now turn to the observed asymmetry of the Stokes and the anti-Stokes peaks in Fig. 2(b). In this experimental configuration $\mathbf{k}_{\text{in}}$ points along the x direction for small incidence angles. This orientation corresponds to a geometry in which the backward volume magnetostatic wave is characterized by symmetrical Stokes—anti-Stokes BLS intensities. When the incidence angle is increased, $\mathbf{k}_{\text{in}}$ rotates toward the y axis, and one has the case of a Damon-Eshbach surface wave. The surface wave is characterized by a high Stokes–anti-Stokes asymmetry associated with the nonreciprocal propagation of these excitations.[12]

V. CONCLUSION

We have examined experimentally and theoretically families of propagating guided modes which exist in metallic magnetic stripes. The modes have continuous wave numbers along the direction of propagation and are quantized in both transverse directions due to confinement.

Experimentally we have shown that these modes can be easily observed using Brillouin light scattering. The theory is an extension of previous work to compute all components of the Green's function of dipole field induced by the dynamic magnetization of the guided modes. We showed how contributions from the total dipole field associated with the guided modes can be identified through analysis of experimental data. Dispersion relations for the cases of longitudinal and transverse magnetization were calculated and features specific to longitudinal guided modes in the long wavelength limit were identified.

ACKNOWLEDGMENTS

This work was supported by the Australian Research Council and the Italian Minister for the Instruction, University and Research (MIUR) is gratefully acknowledged. J.H. thanks the Chinese National Academy for support.

APPENDIX: DERIVATION AND PROPERTIES OF THE GREEN'S FUNCTION

We start with the Green's function of the dipole field induced by an arbitrary three-dimensional profile of magnetization $\mathbf{m}(\boldsymbol{\rho})$

$$\mathbf{h}_d(\boldsymbol{\rho}) = \int_V \hat{G}_V(\boldsymbol{\rho}-\boldsymbol{\rho}')\mathbf{m}(\boldsymbol{\rho}')dV, \tag{A1}$$

where

$$\hat{G}_{V\alpha\alpha'}(\boldsymbol{\rho}-\boldsymbol{\rho}') = \frac{\partial}{\partial\alpha}\frac{\partial}{\partial\alpha'}\frac{1}{|\boldsymbol{\rho}-\boldsymbol{\rho}'|} \tag{A2}$$

[see Eq. (5.98) in Ref. 26], $\boldsymbol{\rho}=(x,y,z)$, $\alpha=x$, y, or z, and V is the sample volume. We specify the shape of the sample as being a rectangle of the infinite length along y having the width w along x and the thickness L along z, such that $p=L/w \ll 1$. We neglect variation of magnetization $\mathbf{m}$ along z and calculate the dipole field associated with wave traveling along y [Eq. (3)].

We substitute the first of Eqs. (3) into Eq. (A1) and integrate over the volume of the rectangle. Finally we average the z-profile of the obtained dipole field inside the stripe over the film thickness. This gives the dependence between $\mathbf{m}_k(x)$ and $\mathbf{h}_{dk}(x)$ from Eqs. (3) in the form of Eq. (4). The kernel $\hat{G}_k(x-x')$ in Eq. (4) is

$$\hat{G}_k(x-x') = \frac{1}{L}\int_{-\infty}^{\infty} dt \int_{-L/2}^{L/2} dz \int_{-L/2}^{L/2} dz' \hat{G}_V(x-x',t,z-z') \times \exp(-ik_y t). \tag{A3}$$

By calculating the integrals over z and z' analytically one obtains Eq. (5).

We note that the out-of-plane diagonal component G_{zzk} was derived in Ref. 24. It can be expressed in terms of modified Bessel functions, as shown:

$$G_{zzk}(s) = 1/(\pi L)[K_0(k\sqrt{s^2+L^2}) - K_0(k_y|s|)]. \tag{A4}$$

Some parts of the other components can also be presented in terms of modified Bessel functions.

In the limit $k_y=0$ the Green's function (5) reduces to the Green's function for WSSWRs from Ref. 23. In particular, one gets $G^0_{zzk}(s)=(1/2\pi L)\ln[s^2/(s^2+L^2)]$. The other important component G_{xxk} in the limit $k_y=0$ reduces to $G_{xxk}(s) = -\delta(s)-G^0_{zzk}(s)$ and G_{yyk} vanishes. In the limit of plane waves in an unconfined film, $w\to\infty$, the components of $\hat{G}_k$ lose their dependence on x and x', and $-G_{yyk}$ becomes the so-called "dipole matrix element" $P_{00}=1-[1-\exp(-k_y L)]/(k_y L)$[27,22] which describes the dipole field of the lowest-order thickness mode in the "diagonal approximation" and has a sense of an effective wave-number-dependent demagnetizing factor for a ferromagnetic film. In this limit the component G_{xxk} vanishes. In the limit of a bulk sample $L,w\to\infty$, the only nonvanishing component is G_{yyk}. This term is responsible for the only component of dipole field in a spin wave which is along the wave propagation direction. It is this component which gives rise to the dependence of bulk spin wave frequency on the propagation angle with respect to the static field (see, e.g., Ref. 28). In the limit of the unconfined film $w\to\infty$ this component describes the increase in frequency of the Damon-Eshbach magnetostatic surface wave with wave number.

The components (5) are singular on the diagonal $x=x'$. However, the integrals of the components over x' are finite. Therefore the functions

$$R_{\alpha\beta k}(x) = 1/w \int_{-w/2}^{w/2} G_{\alpha\beta k}(x,x')dx' \tag{A5}$$

can be used to quantitatively compare the components of $\hat{G}_k$. One can also use the integrals (A5) for estimation of amplitudes of components of the spin-wave dipole field. The latter is possible since $R_{\alpha\beta}(x)$ represents the profile of the α component of the dipole field induced by a homogenous profile of magnetization pointing along the β direction. Furthermore, we note that the profile $\mathbf{m}_k(x)$ of the lowest guided mode is quasihomogeneous (see Fig. 4, lower panel, $n=0$). We also note that for $p \ll 1$ the function $R_{\alpha\alpha k}(x)$ does not noticeably differ from a constant unless in the areas of length of order L at the stripe edges. (This reflects the fact that the dipole field profile of a homogeneous magnetization is quasihomogeneous.) Then an estimate of the dispersion law for the lowest guided mode can be obtained from Eq. (6) setting $m_{k\alpha}(x) \cong m_{k\alpha}(0)$ and replacing the integrals by $R_{\alpha\alpha k}(0)m_{k\alpha}(0)$, where $x=0$ corresponds to the middle of the stripe width. This transforms the system of integrodifferential equations (6) into an algebraic equation. For instance, for the geometry of Fig. 1(a) one gets

$$\omega^2(k) = \{\gamma^2 H_i^2 - 4\pi M_S[R_{zzk}(0) + R_{xxk}(0)] + (4\pi M_S)^2 R_{zzk}(0)R_{xxk}(0)\}. \tag{A6}$$

Figure 5 shows the dependencies $-1+R_{xxk}(0)$ and $R_{zzk}(0)$ on k_y. One sees that for $p<1$ $|R_{zzk}|$ is larger and has a stronger dependence on k_y than $|R_{xxk}|$. This is not unexpected, since G_{xxk} does not vanish only due to confinement in the transverse direction. It gradually decreases with a decrease in p. Provided $p \ll 1$, the transverse confinement is not important for large longuitudinal wave numbers $k_y \gg \pi/w$, therefore in this limit R_{xxk} is vanishing. On the other hand, as long as k_y is not much larger than $1/L$ the components R_{zzk} and R_{yyk} remain k_y dependent, as in this limit they tend to $-P_{00}$ and $-1+P_{00}$, respectively.

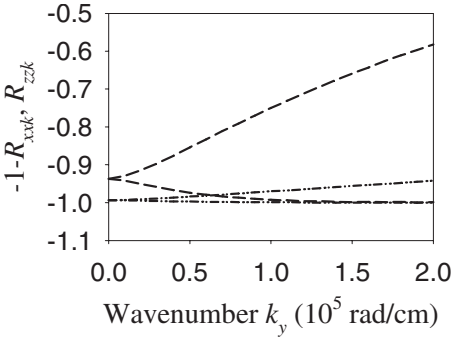

FIG. 5. Components of the tensorial Green's function (3) integrated over the stripe width [Eq. (A6) in the Appendix]. Dashed lines are for $p=0.1$ and dashed-dotted lines are for $p=0.01$. Lines with a positive slope: the zz component, lines with a negative slope: the xx component. Values for R_{yyk} are the difference between the lines for $-1+R_{xxk}$ and R_{zzk}.

The relation $|R_{zzk}| > |R_{xxk}|$ results in a negative dispersion of guided modes [Eq. (A5)] in the geometry of Fig. 1(a), since this case only involves G_{zzk} and G_{xxk}, and as $|R_{zzk}|$ decreases with increasing k_y. The numerical calculation in Fig. 3 is in agreement with this conclusion. In the case of Fig. 1(b), the two components G_{zzk} and G_{yyk} are involved and each has a similar dependence on k_y. However, the slope of G_{zzk} with respect to k_y is negative and the slope of G_{yyk} with respect to k_y is positive. This results in a competition of dipole energies associated with these components and the dispersion of guided modes in this case is more complicated (see Fig. 4).

[1] R. Hertel, W. Wulfhekel, and J. Kirschner, Phys. Rev. Lett. **93**, 257202 (2004).
[2] M. P. Kostylev, A. A. Serga, T. Schneider, B. Leven, and B. Hillebrands, Appl. Phys. Lett. **87**, 153501 (2005).
[3] M. Bailleul, D. Olligs, C. Fermon, and S. O. Demokritov, Europhys. Lett. **56**, 741 (2001).
[4] W. K. Hiebert, G. E. Ballentine, and M. R. Freeman, Phys. Rev. B **65**, 140404(R) (2002).
[5] B. Hillebrands, in *Novel Techniques for Characterizing Magnetic Materials*, edited by Yimey Zhu (Springer, New York, 2005).
[6] C. Mathieu, J. Jorzick, A. Frank, S. O. Demokritov, A. N. Slavin, B. Hillebrands, B. Bartenlian, C. Chappert, D. Decanini, F. Rousseaux, and E. Cambril, Phys. Rev. Lett. **81**, 3968 (1998).
[7] C. Bayer, S. O. Demokritov, B. Hillebrands, and A. N. Slavin, Appl. Phys. Lett. **82**, 607 (2003).
[8] N. A. Sergeeva, S.-M. Chérif, A. Stachkevitch, M. Kostylev, and Y. Roussigné, Phys. Status Solidi C **1**, 1587 (2004).
[9] G. Gubbiotti, M. Kostyleva, N. Sergeevaa, M. Conti, G. Carlotti, T. Ono, A. N. Slavin, and A. Stashkevich, Phys. Rev. B **70**, 224422 (2004).
[10] G. Gubbiotti, G. Carlotti, T. Ono, and Y. Roussigne, J. Appl. Phys. **100**, 023906 (2006).
[11] C. Bayer, J. Jorzick, B. Hillebrands, S. O. Demokritov, R. Kouba, R. Bozinoski, A. N. Slavin, K. Guslienko, D. Berkov, N. Gorn, and M. P. Kostylev, Phys. Rev. B **72**, 064427 (2005).
[12] R. W. Damon and J. R. Eshbach, J. Phys. Chem. Solids **19**, 308 (1961).
[13] B. A. Kalinikos, N. V. Kozhus, M. P. Kostylev, and A. N. Slavin, J. Phys.: Condens. Matter **2**, 9861 (1990).
[14] M. P. Kostylev, A. A. Stashkevich, and N. A. Sergeeva, Phys. Rev. B **69**, 064408 (2004).
[15] G. Gubbiotti, S. Tacchi, G. Carlotti, P. Vavassori, N. Singh, S. Goolaup, A. O. Adeyeye, A. Stashkevich, and M. Kostylev, Phys. Rev. B **72**, 224413 (2005).
[16] G. Gubbiotti, S. Tacchi, G. Carlotti, N. Singh, S. Goolaup, A. O. Adeyeye, and M. Kostylev, Appl. Phys. Lett. **90**, 092503 (2007).
[17] J. R. Sandercock, in *Light Scattering in Solids III*, edited by M. Cardona and G. Güntherodt (Springer-Verlag, Berlin, 1982), p. 173.

[18] M. Koshiba and Y. Long, IEEE Trans. Microwave Theory Tech. **37**, 1768 (1989).
[19] R. Arias and D. L. Mills, Phys. Rev. B **70**, 094414 (2004).
[20] M. Kostylev, J.-G. Hu, and R. L. Stamps, Appl. Phys. Lett. **90**, 012507 (2007).
[21] T. W. O'Keefe and R. W. Patterson, J. Appl. Phys. **49**, 4886 (1978).
[22] B. A. Kalinikos and A. N. Slavin, J. Phys. C **19**, 7013 (1986).
[23] K. Yu. Guslienko, S. O. Demokritov, B. Hillebrands, and A. N. Slavin, Phys. Rev. B **66**, 132402 (2002).
[24] K. Yu. Guslienko, V. Pishko, V. Novosad, K. Buchanan, and S. D. Bader, J. Appl. Phys. **97**, 10A709 (2005).
[25] K. Yu. Guslienko, and A. N. Slavin, Phys. Rev. B **72**, 014463 (2005).
[26] J. D. Jackson, *Classical Electrodynamics* (Wiley, New York, 1975).
[27] B. A. Kalinikos, IEE Proc., Part H: Microwaves, Opt. Antennas **127**, 4 (1980).
[28] A. G. Gurevich and G. A. Melkov, *Magnetization Oscillations and Waves* (CRC Press, New York, 1996).